Proceedings of the 45th IEEE Conference on Decision & Control
Manchester Grand Hyatt Hotel
San Diego, CA, USA, December 13-15, 2006

Nonlinear control for systems with bounded inputs: Real-time embedded control applied to UAVs

Farid Kendoul, David Lara, Isabelle Fantoni and Rogelio Lozano

Abstract— **In this paper, we propose a nonlinear controller for the stabilization of a rotary-wing aircraft class. The control strategy is based on nested saturation technique which results in uncoupled and explicitly-given inputs. The introduction of positive gains in the control law has permitted to take into account the coupling terms, and to improve the dynamical performance of the closed-loop system especially the convergence speed. The controller performances have been confirmed in simulations when we have compared this approach with other existing controllers. We also present the testbed and the implementation of the control law on a quadrirotor aircraft. Using embedded sensors and onboard control, we performed a real-time autonomous flight. Indeed, experimental results have shown that the proposed control strategy is able to perform autonomously the tasks of taking-off, hovering and landing.**

I. INTRODUCTION

In the last decade, a significant progress toward autonomous aerial vehicles with onboard intelligent capabilities has occurred. These systems open new applications in the field of robotics including surveillance, disaster (environmental, industrial and urban) remediation, search, rescue and many others.

Recently, many different Vertical Take-Off and Landing (VTOL) UAVs including conventional helicopters, four-rotors aircraft (Draganflyer) and several designs such as the Guardian from Bombardier, and the Sikorksy Cypher or DragonWarrior have appeared and have been extensively studied. The main advantage of helicopters and other VTOL platforms is the manoeuvrability, needed for many robotic applications.

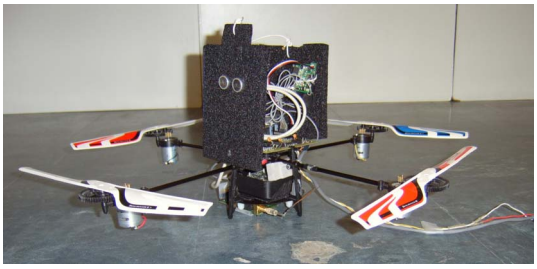

Fig. 1. The modified Draganflyer rotorcraft

When designing control laws for small aerial vehicles, some restrictions and conditions specific to small UAVs have to be considered. First, saturation nonlinearities are particulary prevalent, where actuator saturation has a significant effect on the overall stability of the aircraft. Furthermore, onboard or embedded microprocessors have a limited computational power, so that control algorithms have to be simple and easy to implement and to compute with minimum nonlinear terms.

Several new nonlinear tools have been introduced for analyzing and controlling linear and nonlinear systems with saturation [1], [2]. One of the fundamental method is *the Nested saturation technique* proposed by Teel [3]. Exploiting this technique, Castillo *et al.* [4] have proposed a strategy to stabilize a four-rotors mini-helicopter with bounded inputs. They have considered that the quadrirotor is composed of two independent PVTOLs. The control strategy aimed to stabilize the altitude z, then the first PVTOL ($\phi - y$ displacement) and finally, to control the second PVTOL ($\theta - x$ movement) without taking into account the coupling between these three subsystems [4], [5]. Moreover, the convergence speed of the closed-loop dynamics turns out to be very slow.

The present paper extends previous works from [4], [5]. The main contributions are first to prove the global asymptotic stability of the complete model of rotary-wing aircraft category, considering the coupling between the PVTOLs and the influence of the altitude movement control on the horizontal (longitudinal and lateral) displacement. We also provide convergence analysis for a large range of saturation levels. This allows us to have more flexibility in the adjustment of the controller and to reduce the time of convergence. Moreover, some positive gains have been added in the control law in order to improve the convergence speed of the closed-loop system, and to guarantee the robustness against the nonlinear coupling terms. In addition, a real-time application with embedded control (embedded sensors for position and attitude measurement and onboard microprocessor for control inputs computing) has also been provided.

In Section II, we present the nonlinear model of a class of aerial vehicles. Section III considers the stabilization problem, and the convergence analysis of the closed-loop system is presented in Section IV. The dynamical performance of the proposed control law are compared in simulations to those of [4] and the simulation results are shown in Section V. Section VI is devoted to the testbed description and experiment setup. The paper ends with some conclusions in Section VII.

II. ROTORCRAFT'S NONLINEAR MODEL

Modeling the UAV dynamics is a main issue [6]. In most cases, the aerial robot is considered as a rigid body which is subject to body force $F \in \mathbb{R}^3$ and torque $\tau \in \mathbb{R}^3$, applied

This work was supported by the French Picardie Region Council
The authors are with the Heudiasyc laboratory, UMR CNRS 6599, Université de Technologie de Compiègne, 60200 Compiègne, France {fkendoul,dlara,ifantoni,rlozano}@hds.utc.fr

to its center of mass and specified with respect to the body coordinate frame $\mathcal{B} = (E_1, E_2, E_3)$. Then, the equations of motion are given by the following Newton-Euler equations in the inertial frame $\mathcal{I} = (E_x, E_y, E_z)$ [7], [8], [9], [10]

$$\begin{cases} m\ddot{\xi} = RF - mgE_z \\ J\dot{\Omega} + \Omega \times J\Omega = \tau \end{cases} \quad (1)$$

where $\xi = (x, y, z) \in \mathbb{R}^3$ is the position of the center of gravity with respect to the inertial frame $\mathcal{I}$. $m \in \mathbb{R}$ specifies the mass, and $J \in \mathbb{R}^{3\times3}$ is an inertial matrix expressed in $\mathcal{B}$. The body angular velocity vector $\Omega \in \mathbb{R}^3$ is also expressed in the local frame $\mathcal{B}$. g represents the gravitational constant and $R \in SO(3)$ is the rotational matrix of the body axes relative to the spatial axes. R can be obtained using Euler angles, $\eta = (\phi, \theta, \psi)$ which are respectively the roll, pitch and yaw:

$$R = \begin{pmatrix} c_\theta c_\psi & c_\theta s_\psi & -s_\theta \\ s_\phi s_\theta c_\psi - c_\phi s_\psi & s_\phi s_\theta s_\psi + c_\phi c_\psi & s_\phi c_\theta \\ c_\phi s_\theta c_\psi + s_\phi s_\psi & c_\phi s_\theta s_\psi - s_\phi c_\psi & c_\phi c_\theta \end{pmatrix} \quad (2)$$

Note that s and c represent the $sine$ and $cosine$ functions, respectively.

Let us recall the kinematic relationship between the generalized velocities $\dot{\eta} = (\dot{\phi}, \dot{\theta}, \dot{\psi})$ and the angular velocity Ω

$$\Omega = W\dot{\eta} \quad (3)$$

The expression of the matrix $W \in \mathbb{R}^{3\times3}$ can be found in [8], [9].

In order to exploit the nested saturation technique, we will transform system (1) in a suitable structure. First, substituting (3) into (1), we obtain

$$\begin{cases} m\ddot{\xi} = RF - mgE_z \\ JW\ddot{\eta} + J\dot{W}\dot{\eta} + W\dot{\eta} \times JW\dot{\eta} = \tau \end{cases} \quad (4)$$

Defining a pseudo-inertial matrix $\mathbb{I}(\eta) = JW$ and a coriolis/centripetal vector $C(\dot{\eta}, \eta) = \dot{\mathbb{I}}\dot{\eta} + W\dot{\eta} \times \mathbb{I}\dot{\eta}$, system (4) can be written in the form

$$\begin{cases} m\ddot{\xi} = RF - mgE_z \\ \mathbb{I}(\eta)\ddot{\eta} + C(\dot{\eta}, \eta) = \tau \end{cases} \quad (5)$$

Now, we will focus our study on the model of a rotorcraft vehicle which is characterized by three control torques $\tau = (\tau_\phi, \tau_\theta, \tau_\psi)^T$ and only the vertical component of the force vector $F = (0, 0, u)^T$. Then, by recalling (5), the dynamics of this four-rotor rotorcraft is governed by the system

$$m\ddot{\xi} = u \begin{pmatrix} -s_\theta \\ s_\phi c_\theta \\ c_\phi c_\theta \end{pmatrix} + \begin{pmatrix} 0 \\ 0 \\ -mg \end{pmatrix} \quad (6)$$

$$\mathbb{I}(\eta)\ddot{\eta} = \tau - C(\dot{\eta}, \eta) \quad (7)$$

The analytical expressions of the four control inputs $(u, \tau_\phi, \tau_\theta, \tau_\psi)$ can be found in [4], [11].

III. STABILIZATION WITH BOUNDED INPUTS

We first transform system (6)-(7) by proposing the following change of input variables

$$\tau = C(\eta, \dot{\eta}) + \mathbb{I}\tilde{\tau}, \text{ where } \tilde{\tau} = (\tilde{\tau}_\phi, \tilde{\tau}_\theta, \tilde{\tau}_\psi)^T \quad (8)$$

are the new inputs. Therefore, the rotary-wing aircraft model can be represented by the following system

$$\begin{cases} m\ddot{x} = -u\sin\theta \\ m\ddot{y} = u\cos\theta.\sin\phi \\ m\ddot{z} = u\cos\theta.\cos\phi - mg \\ \ddot{\phi} = \tilde{\tau}_\phi,\ \ddot{\theta} = \tilde{\tau}_\theta,\ \ddot{\psi} = \tilde{\tau}_\psi \end{cases} \quad (9)$$

We notice that this system can be divided into four coupled subsystems, each one controlled by a single input .

In the following, we will construct a nonlinear controller for each subsystem, and we will prove that the proposed control law takes into account the coupling terms connecting these subsystems. Indeed, we consider the effects of coupling terms as disturbances. Thus, we propose a decoupled control design and provide a complete stability analysis of the closed-loop system.

A. YAW AND ALTITUDE CONTROL

The yaw dynamics is governed by the following double integrator: $\ddot{\psi} = \tilde{\tau}_\psi$. Using the nested saturation method [3], it can be proved that the control law

$$\tilde{\tau}_\psi = -\sigma_{\psi1}(k_{\psi1}\dot{\psi} + \sigma_{\psi2}(k_{\psi2}\dot{\psi} + k_{\psi1}\,k_{\psi2}(\psi - \psi_d))) \quad (10)$$

will stabilize the yaw angle at its desired value ψ_d if the positive gains $(k_{\psi1}, k_{\psi2})$ are appropriately chosen (see [12] for more details). $\sigma(.)$ is a linear saturation function which is Lipchitz, nondecreasing and defined as
$\sigma_{\psi i}(x) = sign(x)\ \min(|x|, \psi i),\ i = 1, 2$ and ψi is a real positive constant.

Now, we consider the equation describing the altitude dynamics: $m\ddot{z} = u\cos\theta\cos\phi - mg$. First, we apply a feedback linearization [5] by assigning

$$u = \frac{mr + mg}{\cos\sigma_p(\theta)\cos\sigma_p(\phi)} \quad (11)$$

where $0 < p < \pi/2$. We assume that after a finite time, both $\theta(t)$ and $\phi(t)$ belong to the interval $I_{\pi/2} = (-\frac{\pi}{2} + \epsilon, \frac{\pi}{2} - \epsilon)$ for some $\epsilon > 0$, so that $\cos\theta.\cos\phi \neq 0$.

Then, we obtain a double integrator system: $\ddot{z} = r$ with r is the new input. As for the yaw control, we choose

$$r = -\sigma_{r1}(k_{r1}\dot{z} + \sigma_{r2}(k_{r2}\dot{z} + k_{r1}\,k_{r2}(z - z_d))) \quad (12)$$

B. HORIZONTAL MOVEMENT CONTROL (θ−x and ϕ−y)

After replacing u by its expression in (11), the remaining dynamics is given by

$$\begin{cases} \ddot{x} = -\dfrac{r + g}{\cos\phi}\tan\theta,\ \ \ddot{\theta} = \tilde{\tau}_\theta \\ \ddot{y} = (r + g)\tan\phi,\ \ \ddot{\phi} = \tilde{\tau}_\phi \end{cases} \quad (13)$$

System (13) can be seen as two feedforward subsystems ($x - \theta$ and $y - \phi$) coupled by the term $\cos\phi$ and controlled

by $\tilde{\tau}_\theta$ and $\tilde{\tau}_\phi$, respectively. The variable r can be considered as a bounded ($|r| \leqslant r_1$) perturbation for system (13).

NOTATIONS AND DEFINITIONS: We note $|X| \in \mathbb{R}^n$ a positive vector which is composed of the absolute value of each component, i.e., $|X| = (|x_1|, |x_2|, ..., |x_n|)^T$. In the following sections, for $|X| \in \mathbb{R}^n$ and $|Y| \in \mathbb{R}^n$, the notation $|X| > (<) |Y|$ means that $|x_i| > (<) |y_i|, \ \forall i \in \{1, 2, ..., n\}$.

We note $\tilde{\xi} = (x, y)^T$ the position vector and $\tilde{\eta} = (\theta, \phi)^T$ denotes the orientation vector.

We define a vectorial saturation function $\sigma_a : \mathbb{R}^2 \to \mathbb{R}^2$ as

$$\sigma_a(X) = (\sigma_{a_1}(x_1), \sigma_{a_2}(x_2))^T, \text{ with } a = (a_1, a_2)^T.$$

Using these notations, system (13) can be written in the form

$$\begin{cases} \ddot{\tilde{\xi}} = A\tilde{\eta} + D(\tilde{\eta}, r) \\ \ddot{\tilde{\eta}} = \nu \end{cases} \tag{14}$$

where

$$A = \begin{pmatrix} -g & 0 \\ 0 & g \end{pmatrix}, \ \nu = (\tilde{\tau}_\theta, \tilde{\tau}_\phi)^T$$

and

$$D(\tilde{\eta}, r) = \begin{pmatrix} -(r+g)\frac{\tan\theta}{\cos\phi} + g\theta \\ (r+g)\tan\phi - g\phi \end{pmatrix} \tag{15}$$

System (14) can be seen as a chain of four integrators according to the variables $\tilde{\xi}$ and $\tilde{\eta}$ which is perturbed by the nonlinear function $D(\tilde{\eta}, r)$.

Thus, the control law (ν) will be constructed recursively in four steps. The key idea is to bound each variable successively starting by ($\dot{\tilde{\eta}}$).

STEP 1: BOUNDEDNESS OF $\dot{\tilde{\eta}}$

We first examine the trajectory of $\dot{\tilde{\eta}}$. We recall: $\ddot{\tilde{\eta}} = \nu$. Let us define V_1, a positive definite function: $V_1 = \frac{1}{2}\dot{\tilde{\eta}}^T\dot{\tilde{\eta}} = \frac{1}{2}\dot{\theta}^2 + \frac{1}{2}\dot{\phi}^2$, whose time derivative may be written as

$$\dot{V}_1 = \dot{\tilde{\eta}}^T\ddot{\tilde{\eta}} = \dot{\tilde{\eta}}^T\nu \tag{16}$$

The input ν is chosen as follows

$$\nu = -\sigma_a(K_1\dot{\tilde{\eta}} + \sigma_b(\nu_1)) \tag{17}$$

where $\nu_1 \in \mathbb{R}^2$ is the new input which will be assigned in the next step. In the sequel, the matrices K_i $(i = 1, ..., 4) \in \mathbb{R}^{2\times 2}$ are diagonal and composed of positive constants k_{i_θ} and k_{i_ϕ}.

Now, we have: $\dot{V}_1 = -\dot{\tilde{\eta}}^T\sigma_a(K_1\dot{\tilde{\eta}} + \sigma_b(\nu_1))$.

It is clear that if $|K_1\dot{\tilde{\eta}}| > b$ then $\dot{V}_1 < 0$, and $\dot{\tilde{\eta}}$ will decrease until it reaches the domain of attraction $Q_1 = [-|K_1^{-1}b|, |K_1^{-1}b|]$ in a finite time T_1.

$$|\dot{\tilde{\eta}}| \leqslant |K_1^{-1}b| \tag{18}$$

If we choose $b \leqslant \frac{1}{2}a$, then σ_a will operate in its linear region for all $t \geqslant T_1$. Thus, $\ddot{\tilde{\eta}} = \nu = -K_1\dot{\tilde{\eta}} - \sigma_b(\nu_1)$, which implies

$$\ddot{\tilde{\eta}} + K_1\dot{\tilde{\eta}} = -\sigma_b(\nu_1) \tag{19}$$

STEP 2: BOUNDEDNESS OF $\tilde{\eta}$

Now, we consider the new system in (19) with the new input ν_1. By defining a new variable z_2 such as

$$z_2 = \dot{\tilde{\eta}} + K_1\tilde{\eta} \tag{20}$$

then we have $\dot{z}_2 = -\sigma_b(\nu_1)$. Next, by choosing

$$\nu_1 = K_2 z_2 + \sigma_c(\nu_2) \tag{21}$$

The time derivative of z_2 is now given by

$$\dot{z}_2 = -\sigma_b(K_2 z_2 + \sigma_c(\nu_2)) \tag{22}$$

which is similar to $\ddot{\tilde{\eta}}$ in (14) and (17). As previously, we define a positive definite function V_2 as: $V_2 = \frac{1}{2}z_2^T z_2$. Then, $\dot{V}_2 = -z_2^T\sigma_b(K_2 z_2 + \sigma_c(\nu_2))$.

The control law (21) forces the variable z_2 to converge to its domain of attraction in a finite time $T_2 \geqslant T_1$, i.e.,

$$|K_2 z_2| \leqslant c, \quad \forall t \geqslant T_2 \tag{23}$$

By setting $c \leqslant \frac{1}{2}b$, system (22) becomes:
$\dot{z}_2 + K_2 z_2 = -\sigma_c(\nu_2)$.

Since z_2 is bounded $\forall t \geqslant T_2$, the boundedness of $\tilde{\eta}$ ($\tilde{\eta} \in Q_{\tilde{\eta}}$) can be deduced by solving the differential equation in (20). We thus find (see [5])

$$|\tilde{\eta}| \leqslant K_2^{-1}c, \quad \forall t \geqslant T_3 \geqslant T_2 \tag{24}$$

Notice that $Q_{\tilde{\eta}}$ depends on c and K_2. Therefore, the parameters (c, K_2) can be chosen to guarantee that $\tilde{\eta} \in I_{\pi/2} \times I_{\pi/2}$ for all $t \geqslant T_3$.

STEP 3: BOUNDEDNESS OF $\dot{\tilde{\xi}}$

Let us recall that

$$\begin{cases} \ddot{\tilde{\xi}} = A\tilde{\eta} + D(\tilde{\eta}, r) \\ \dot{z}_2 + K_2 z_2 = -\sigma_c(\nu_2), \ z_2 = \dot{\tilde{\eta}} + K_1\tilde{\eta} \end{cases} \tag{25}$$

We define a new variable z_3 as follows

$$z_3 = z_2 + K_2\tilde{\eta} + K_2K_1A^{-1}\dot{\tilde{\xi}} \tag{26}$$

Differentiating the above equation, we obtain

$$\dot{z}_3 = -\sigma_c(\nu_2) + K_2K_1A^{-1}D(\tilde{\eta}, r) \tag{27}$$

The input ν_2 of this system is selected as: $\nu_2 = K_3 z_3 + \sigma_d(\nu_3)$. Define a new positive definite function: $V_3 = \frac{1}{2}z_3^T z_3$. The time derivative of V_3 can be written in the form

$$\dot{V}_3 = -z_3^T[\sigma_c(K_3 z_3 + \sigma_d(\nu_3)) - K_2K_1A^{-1}D(\tilde{\eta}, r)]$$

Using a similar analysis, it can be shown that after a finite time $T_4 \geqslant T_3$, the variable z_3 satisfies

$$|K_3 z_3| \leqslant d + K_2K_1M \tag{28}$$

where $M \in \mathbb{R}^2$ is positive vector and is defined as follows (see [11] for its explicit expression and more details).

$$M = \max_{(\tilde{\eta} \in Q_{\tilde{\eta}})}|A^{-1}D(\tilde{\eta}, r)| \tag{29}$$

From (23), (24), (26) and (28), we can show that $\dot{\tilde{\xi}}$ is bounded.

If the saturation level c is chosen such that it satisfies

$$c \geqslant 2d + K_2K_1M$$

Then, $\dot{z}_3$ in (27) is given by

$$\dot{z}_3 + K_3z_3 = -\sigma_d(\nu_3) + K_2K_1A^{-1}D(\tilde{\eta}, r) \quad (30)$$

STEP 4: BOUNDEDNESS OF $\tilde{\xi}$

Finally, the input ν_3 is chosen as follows

$$\nu_3 = K_4(z_3 + K_3\tilde{\eta} + K_3(K_1+K_2)A^{-1}\dot{\tilde{\xi}} + K_3K_2K_1A^{-1}\tilde{\xi}) \quad (31)$$

This choice is motivated by the fact that using (25), (26) and (30), $\dot{\nu}_3$ can now be expressed as

$$\dot{\nu}_3 = -K_4[\sigma_d(\nu_3) - (K_3K_1 + K_3K_2 + K_2K_1)A^{-1}D(\tilde{\eta}, r)] \quad (32)$$

Let us define V_4 a positive definite function given by: $V_4 = \frac{1}{2}\nu_3^T\nu_3$. $\dot{V}_4$ is therefore,

$$\dot{V}_4 = -\nu_3^TK_4[\sigma_d(\nu_3) - (K_3K_1 + K_3K_2 + K_2K_1)A^{-1}D(\tilde{\eta}, r)]$$

If $d \geqslant (K_3K_1 + K_3K_2 + K_2K_1)M$, then after a finite time T_5, we obtain

$$|\nu_3| \leqslant (K_3K_1 + K_3K_2 + K_2K_1)M \leqslant d \quad (33)$$

Therefore, (32) leads to

$$\dot{\nu}_3 + K_4\nu_3 = K_4(K_3K_1 + K_3K_2 + K_2K_1)A^{-1}D(\tilde{\eta}, r) \quad (34)$$

Since $\dot{\tilde{\xi}}$, $\tilde{\eta}$, z_3 and ν_3 are bounded $\forall t \geqslant T_5$, we obtain from (31) that $\tilde{\xi}$ is bounded, and all the saturation functions will operate in their linear regions for all $t \geqslant T_5$.

IV. CONVERGENCE ANALYSIS

In this section, we will prove that all the states converge to zero even in the presence of the nonlinear coupling term $D(\tilde{\eta}, r)$. The global asymptotic stability is ensured by a convenient choice of the saturation level c and the gains K_i.

Equation (34) can be written as follows

$$\dot{\nu}_3 + K_4\nu_3 = KA^{-1}D(\tilde{\eta}, r) \quad (35)$$

with $K = K_4(K_3K_1 + K_3K_2 + K_2K_1)$.

The vector $A^{-1}D(\tilde{\eta}, r)$ can be subdivided into two terms: $H(\tilde{\eta})$ which depends only on the state vector $\tilde{\eta}$, and $R(\tilde{\eta}, r)$ which is function of $\tilde{\eta}$ and r. These vectors can be computed from (15) and expressed as below

$$H(\tilde{\eta}) = (\frac{\tan\theta}{\cos\phi} - \theta, \tan\phi - \phi)^T \ , \ R(\tilde{\eta}, r) = (\frac{r\tan\theta}{g\cos\phi}, \frac{r\tan\phi}{g})^T \quad (36)$$

Now, (35) can be written in the form

$$\dot{\nu}_3 + K_4\nu_3 = KH(\tilde{\eta}) + KR(\tilde{\eta}, r)$$

After analyzing the above differential equation, we found that its solution satisfies the inequality below for all $\tilde{\eta} \in Q_{\tilde{\eta}}$

$$|\nu_3| \leqslant K|H(\tilde{\eta})| + K|R(\tilde{\eta}, r)| \quad (37)$$

From (30), we also have

$$\dot{z}_3 + K_3z_3 = -\nu_3 + K_2K_1H(\tilde{\eta}) + K_2K_1R(\tilde{\eta}, r)$$

Similarly, $|z_3| \leqslant (K + K_2K_1)(|H(\tilde{\eta})| + |R(\tilde{\eta}, r)|)$.

Since $\nu_2 = K_3z_3 + \nu_3$ (see step 3), this implies that

$$|\nu_2| \leqslant (K + K_3(K + K_2K_1))(|H(\tilde{\eta})| + |R(\tilde{\eta}, r)|) \quad (38)$$

For simplicity, let us note $K_0 = (K + K_3(K + K_2K_1))$ which is a diagonal matrix in $\mathbb{R}^{2\times2}$.

From (25), we also deduce that $|z_2| \leqslant K_0|H(\tilde{\eta})| + K_0|R(\tilde{\eta}, r)|$.

Finally, the solution of the differential equation in (20) satisfies also

$$|\tilde{\eta}| \leqslant K_0|H(\tilde{\eta})| + K_0|R(\tilde{\eta}, r)| \quad (39)$$

Now, we will prove that $\tilde{\eta}$ will converge to zero if the saturation level c is selected sufficiently small. By recalling (24), (36) and (39), one may write

$$\begin{cases} |\theta| - k_{0_\theta}|\frac{\tan\theta}{\cos\phi} - \theta| \leqslant k_{0_\theta}|\frac{r\tan\theta}{g\cos\phi}|, \ k_{2_\theta}|\theta| \leqslant c_\theta \\ |\phi| - k_{0_\phi}|\tan\phi - \phi| \leqslant k_{0_\phi}|\frac{r\tan\phi}{g}|, \ k_{2_\phi}|\phi| \leqslant c_\phi \end{cases} \quad (40)$$

Let us notice that $(\frac{\tan\theta}{\cos\phi})$ and θ have the same sign (*this result holds since* $|\phi| < \frac{\pi}{2}$), and we can easily verify that $|\tan\theta| \geqslant |\theta|$ which implies $|\frac{\tan\theta}{\cos\phi}| \geqslant |\theta|$ since $0 < \cos\phi \leqslant 1$. These remarks remain valid for the third inequality in (40) with the variable ϕ.

We conclude from these remarks that

$$|\frac{\tan\theta}{\cos\phi} - \theta| = \frac{|\tan\theta|}{\cos\phi} - |\theta| \ , \ |\tan\phi - \phi| = |\tan\phi| - |\phi| \quad (41)$$

Furthermore, we have $k_{2_\phi}|\phi| \leqslant c_\phi$, then $\cos(c_\phi/k_{2_\phi}) \leqslant \cos\phi \leqslant 1 \ \Rightarrow \ 1 \leqslant \frac{1}{\cos\phi} \leqslant \frac{1}{\cos(c_\phi/k_{2_\phi})}$

Substituting (41) in (40) and using the above inequality, we obtain

$$\begin{cases} (1 + k_{0_\theta})|\theta| - k_{0_\theta}\frac{\tan|\theta|}{\cos(c_\phi/k_{2_\phi})} \leqslant k_{0_\theta}|r|\frac{\tan|\theta|}{g\cos\phi}, \ k_{2_\theta}|\theta| \leqslant c_\theta \\ (1 + k_{0_\phi})|\phi| - k_{0_\phi}\tan|\phi| \leqslant k_{0_\phi}|r|\frac{\tan|\phi|}{g}, \ k_{2_\phi}|\phi| \leqslant c_\phi \end{cases} \quad (42)$$

Let us note L_θ the limit of $|\theta|$ when the time goes to infinity, and L_ϕ is the limit of $|\phi|$. Since from (12) $\lim_{t\to\infty} r = 0$ and since the functions $(\frac{\tan|\theta|}{g\cos\phi} \ , \ \frac{\tan|\phi|}{g})$ are bounded, we obtain from (42)

$$\begin{cases} (1 + k_{0_\theta})L_\theta - k_{0_\theta}\frac{\tan L_\theta}{\cos(c_\phi/k_{2_\phi})} \leqslant 0, \ 0 \leqslant k_{2_\theta}L_\theta \leqslant c_\theta \\ (1 + k_{0_\phi})L_\phi - k_{0_\phi}\tan L_\phi \leqslant 0, \ 0 \leqslant k_{2_\phi}L_\phi \leqslant c_\phi \end{cases} \quad (43)$$

Now, it remains to solve the algebraic system (43) for the variables (L_θ, L_ϕ) and to choose the saturation levels (c_θ, c_ϕ) sufficiently small in order to obtain $(L_\theta, L_\phi) = (0, 0)$.

By studying and plotting the inequality "$(1 + k_{0_\phi})L_\phi - k_{0_\phi}\tan L_\phi \leqslant 0, \ L_\phi \in \mathbb{R}^+$", we find that its solution is $0 \cup [\lambda_\phi, \frac{\pi}{2}[$, where λ_ϕ is a positive constant which depends on k_{0_ϕ}. Therefore, if we choose $c_\phi < k_{2_\phi}\lambda_\phi$ (i.e., $L_\phi < \lambda_\phi$), then the only possible solution is $L_\phi = 0$.

With the same analysis, we show that the solution of "$(1 + k_{0_\theta})L_\theta - k_{0_\theta}\frac{\tan L_\theta}{\cos(c_\phi/k_{2_\phi})} \leqslant 0$" is also $0 \cup [\lambda_\theta, \frac{\pi}{2}[$. λ_θ

is a positive constant which depends on the parameters c_ϕ, k_{2_ϕ} and k_{0_θ}. As previously, there exists a value for c_θ ($c_\theta < k_{2_\theta}\lambda_\theta$) which restricts the solution to zero ($L_\theta = 0$).

Example: If all the gains are set to 1, i.e., $K_i = I_{2\times 2}$ for $i = 1, ..., 4$. Then, we obtain $k_{0_\phi} = k_{0_\theta} = 7$ and $L_\phi = 0$ if $c_\phi \leqslant 0.6$. Furthermore, for any admissible value of c_ϕ, there exists a value for c_θ such that $L_\theta = 0$ (see [11] for more details).

Now, if we choose the gains k_i as shown in table (II), we find that for $(c_\theta, c_\phi) = (0.36, 0.4)$, we obtain $(L_\theta, L_\phi) = (0, 0)$.

Finally, we have shown that the saturation level $c = (c_\theta, c_\phi)^T$ can be chosen in such a way that $\lim_{t\to\infty} \tilde{\eta} = 0$. We deduce from (36) that H and R converge to 0. From (37)-(38), we have that $(\nu_2, \nu_3, z_2, z_3) \to (0, 0, 0, 0)$. From the third equation of (25) we get $\tilde{\dot{\eta}} \to 0$. From (26) and (31), it follows respectively that $\tilde{\dot{\xi}} \to 0$ and $\tilde{\xi} \to 0$.

A. SATURATION LEVELS AND GAINS SELECTION

Let us recall all the constraints on saturation levels

$$\begin{cases} a \geqslant 2b,\ b \geqslant 2c \\ c \geqslant 2d + K_2K_1M \\ d \geqslant (K_2K_1 + K_3K_1 + K_3K_2)M \end{cases} \quad (44)$$

Once the vector c is selected according to the previous analysis ($c_\phi = 0.4$ and $c_\theta = 0.36$), the saturation levels a and b can be computed from (44). From (44), the saturation level d can be chosen from the set of solutions of the below inequality (see [11] for more details).

$$(K_2K_1 + K_3K_1 + K_3K_2)M \leqslant d \leqslant \frac{1}{2}(c - K_2K_1M) \quad (45)$$

The gain matrices K_i are selected by taking into account the following criteria: 1) Obtain large values for c_θ and c_ϕ when resolving the system in (43), 2) satisfy the inequality in (45) when selecting d_θ and d_ϕ and 3) optimize the time response of the closed-loop system.

Considering the three above criteria, a primary analysis lead to the following selection of the matrices K_i:
For $k_{i_\phi} = 0.5$, $i = 1, 2, 3$ and $k_{4_\phi} = 1$, and for $(k_{1_\theta}, k_{2_\theta}, k_{3_\theta}, k_{4_\theta}) = (0.2, 0.5, 0.5, 1.8)$, we obtain $c_\theta = 0.36$ and $c_\phi = 0.4$. Furthermore, if r_1 is (for example) set to 3, then from (45), we obtain

$$0.1141 \leqslant d_\phi \leqslant 0.1810$$
$$0.1555 \leqslant d_\theta \leqslant 0.1627$$

These selections allowed the improvement of the dynamical performances of the closed-loop system (see Figure 2). However, a detailed mathematical analysis is required in order to determine the best values for K_i that give a minimal time response of the system.

Finally, the complete expression of the control law for the horizontal movement is given by

$$\nu = -\sigma_a(K_1\dot{\tilde{\eta}} + \sigma_b(K_2z_2 + \sigma_c(K_3z_3 + \sigma_d(\nu_3)))) \quad (46)$$

The complete and explicit formulae of the two control torques $\tilde{\tau}_\theta$ and $\tilde{\tau}_\phi$ can be obtained by replacing $(\tilde{\eta}, z_2, z_3, \nu_3)$ in (46) by their expressions. Note that $\tilde{\tau}_\theta$ and $\tilde{\tau}_\phi$ are uncoupled.

TABLE I
QUADROTOR MODEL PARAMETERS

parameter	*Value*	*parameter*	*Value*
$m\ [kg]$	1		
$I_x\ [kg.m^2]$	5×10^{-3}	$g\ [m/s^2]$	9.81
$I_y\ [kg.m^2]$	5×10^{-3}	$l\ [m]$	0.22
$I_z\ [kg.m^2]$	9×10^{-3}	μ	3×10^{-6}
$I_r\ [kg.m^2]$	4×10^{-5}	κ	1.5×10^{-7}

V. SIMULATIONS

Before testing the controller on the real system shown in Figure 1, we performed different simulations on Matlab/Simulink using the dynamic model in (5) with the parameters listed in table (I). The initial Euler angles and position are given by $\phi_0 = -0.7$ rad, $\theta_0 = 0.8$ rad, $\psi_0 = 0$ rad, $x_0 = 2$ m, $y_0 = -3$ m and $z_0 = 0$ m. Linear and angular velocities are set to zero, i.e. $\dot{\xi} = \dot{\eta} = (0, 0, 0)^T$. The task was to reach the position $z_d = 1$ m and $\psi_d = 1$ rad and to stabilize the other variables to zero. To explore the performance of the proposed controller, we run simulations for three controllers: the control law given by (10), (12), (46) with gains $K_i = I_{2\times 2}$, $i = 1, 2, ..., 4$ (dashdot line), the same algorithm with different gains (see Table II) (solid line), and the third (dotted curve) represents the results for the previous controller proposed in [4]. One can see that the dynamic of the closed-loop system is improved and that a convenient selection of saturation levels and gains K_i permits to reduce considerably the time response of the system and to obtain satisfactory performance as showed in Figure 2.

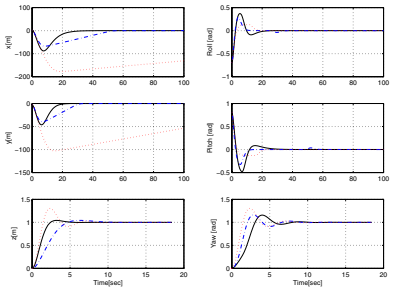

Fig. 2. Position and orientation stabilization

TABLE II
CONTROLLER PARAMETERS

Param.	*Val.*	*Param.*	*Val.*	*Param.*	*Val.*
r_1	3	k_{r1}	1	a_ϕ	1.7
r_2	1.4	k_{r2}	2	b_ϕ	0.82
ψ_1	1.5	$k_{\psi 1}$	1	c_ϕ	0.4
ψ_2	0.7	$k_{\psi 2}$	2	d_ϕ	0.18
a_θ	1.7	k_{1_θ}	0.2	k_{1_ϕ}	0.5
b_θ	0.82	k_{2_θ}	0.5	k_{2_ϕ}	0.5
c_θ	0.36	k_{3_θ}	0.5	k_{3_ϕ}	0.5
d_θ	0.16	k_{4_θ}	1.8	k_{4_ϕ}	1

VI. THE TESTBED AND THE EXPERIMENTAL RESULTS

The UAV platform used in the experiment is a modified Draganflyer III four-rotors helicopter (see Figure 1) manu-

factured by DRAGANFLY Company. In fact, we kept only the airframe, the motors and the blades and added our own sensors and electronic circuitry.

The real-time architecture of the platform shown in Figure 3 includes two microprocessors, a CI3DMGV Microstrain IMU, three ultrasonic sensors, a wireless modem, a Futaba 72 MHz radio, a receiver, power MOSFET and ground station. A microprocessor (Rabbit 3400, 28 MHz) is currently being used as the heart of the control system. A second microcontroller (Pic) is added for the acquisition of the ultrasonic data and estimation of the robot position. These measurements are then sent to the Rabbit via RS232. The Inertial Measurement Unit (IMU) is mounted using a series of elastic bands such that low amplitude, high frequency vibrations of the helicopter could not be transmitted to the sensor. A combination of rate gyros, accelerometers, and magnetometers are used to generate pitch, roll and heading (yaw) estimation at a frequency of 70 Hz. The angular velocities are also available. All filter processing is performed onboard the unit.

The ultrasonic sensors are running at 20 Hz and mounted according to the three axes in order to estimate the position $\xi = (x, y, z)^T$. We have thus computed estimates of linear velocities by using the following approximation $\dot{\xi} = \frac{\xi(t)-\xi(t-T)}{T}$ where T is the sampling period. In our experiment, $T = 0.05s$. Also, both position and linear velocities are filtered using first order low-pass filters.

The communication with the ground station is carried out via 2.4 GHz wireless modem.

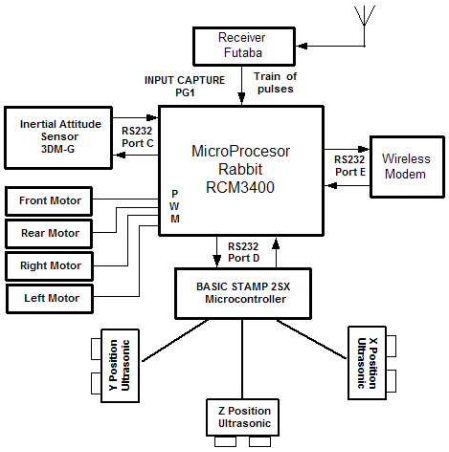

Fig. 3. The real-time architecture of the platform

We mention that the rotorcraft evolves freely in a 3D space without any flying stand, and we have considered an autonomous flight. The objective for the aerial vehicle was to take-off, hover at a desired altitude during a fixed period when stabilizing all the angles and horizontal displacement at zero, and then to land (see Figure 4). We have noticed in the experiment that the control law presented in previous sections is quite robust against parameters uncertainties and external disturbances. Indeed, we have applied external forces to the aircraft during the period 225s - 330s. From Figures 4-5, we notice that the controller rejects these perturbations and that the objective is achieved with a satisfactory performance.

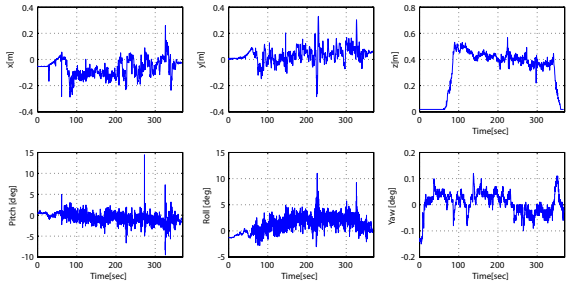

Fig. 4. Autonomous take-off, hovering and landing with external perturbations during the period 225s - 330s

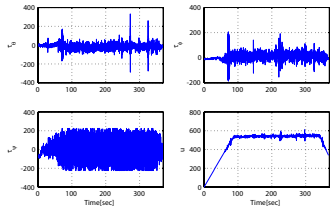

Fig. 5. Control inputs

VII. CONCLUSION

The present paper addresses an effective control strategy for a large class of rotary-wing UAVs. The control law is simple for implementation and results in a very satisfactory performance in practice. We have also described the embedded control system designed and tested in real-time experiment. The results presented in this paper testify to the effectiveness and the good performance of our control system (control law & control architecture).

REFERENCES

[1] T. Lauvdal, R. M. Murray, and T. I. Fossen, "Stabilization of integrator chains in the presence of magnitude and rate saturations: A gain schuduling approach," in *Proceedings of the IEEE CDC*, 1997.

[2] J. H. Sussmann, D. E. Sontag, and Y. Yang, "A general result on the stabilization of linear systems using bounded controls," *IEEE Transactions on Automatic Control*, vol. 39, no. 12, December 1994.

[3] A. Teel, "Global stabilisation and restricted tracking for multiple integrators with bounded controls," *Systems and Control Letters*, vol. 18, pp. 165–171, 1992.

[4] P. Castillo, A. Dzul, and R. Lozano, "Real-time stabilization and tracking of a four rotor mini-rotorcraft," *IEEE Transactions on Control Systems Technology*, vol. 12, no. 4, pp. 510–516, July 2004.

[5] R. Lozano, P. Castillo, and A. Dzul, "Global stabilization of the pvtol: Real-time application to a mini-aircraft," *International Journal of Control*, vol. 77, no. 8, pp. 735–740, May 2004.

[6] R. W. Prouty, *Helicopter performance, stability, and control*, K. P. Compagny, Ed., Malabar, Florida, 1995.

[7] F. Kendoul, I. Fantoni, and R. Lozano, "Modeling and control of a small autonomous aircraft having two tilting rotors," *In Proceedings of the 44th IEEE CDC, and the ECC*, pp. 8144–8149, Seville, Spain December, 2005.

[8] I. Fantoni and R. Lozano, *Non-linear control for underactuated mechanical systems*, ser. Communications and Control Engineering Series, Springer-Verlag, Ed., 2002.

[9] B. Etkin, *Dynamics of Flight*, John Wiley & Sons, Ed., New York, 1959.

[10] B. W. McCormick, *Aerodynamics Aeronautics and Flight Mechanics*, John Wiley & Sons, Ed., New York, 1995.

[11] F. Kendoul, D. Lara, I. Fantoni, and R. Lozano, "Real-time nonlinear embedded control for a quad-rotor helicopter," *Accepted in he Int. J. of Robust and Nonlinear Control*, 2005.

[12] E. N. Johnson and S. K. Kannan, "Nested saturation with guaranteed real poles," Georgia Institute of Technology, Atlanta.